PROPERTIES OF DUST GRAINS PROBED WITH EXTINCTION CURVES

Takaya Nozawa[1] and Masataka Fukugita[1,2,3]
[1] Kavli Institute for the Physics and Mathematics of the Universe (WPI), University of Tokyo, Kashiwa 277-8583, Japan
[2] Institute for Cosmic Ray Research, University of Tokyo, Kashiwa 277-8582, Japan
[3] Institute for Advanced Study, Princeton, NJ 08540, USA

ABSTRACT

Modern data of the extinction curve from the ultraviolet to the near-infrared are revisited to study properties of dust grains in the Milky Way (MW) and the Small Magellanic Cloud (SMC). We confirm that the graphite–silicate mixture of grains yields the observed extinction curve with the simple power-law distribution of the grain size but with a cutoff at some maximal size: the parameters are tightly constrained to be $q = 3.5 \pm 0.2$ for the size distribution a^{-q} and the maximum radius $a_{\max} = 0.24 \pm 0.05\,\mu$m, for both MW and SMC. The abundance of grains, and hence the elemental abundance, is constrained from the reddening versus hydrogen column density, $E(B - V)/N_{\rm H}$. If we take the solar elemental abundance as the standard for the MW, $>56\%$ of carbon should be in graphite dust, while it is $<40\%$ in the SMC using its available abundance estimate. This disparity and the relative abundance of C to Si explain the difference of the two curves. We find that 50%–60% of carbon may not necessarily be in graphite but in the amorphous or glassy phase. Iron may also be in the metallic phase or up to $\sim80\%$ in magnetite rather than in silicates, so that the Mg/Fe ratio in astronomical olivine is arbitrary. With these substitutions, the parameters of the grain size remain unchanged. The mass density of dust grains relative to hydrogen is $\rho_{\rm dust}/\rho_{\rm H} = 1/(120^{+10}_{-16})$ for the MW and $1/(760^{+70}_{-90})$ for the SMC under the elemental abundance constraints. We underline the importance of the wavelength dependence of the extinction curve in the near-infrared in constructing the dust model: if $A_\lambda \propto \lambda^{-\gamma}$ with $\gamma \simeq 1.6$, the power-law grain-size model fails, whereas it works if $\gamma \simeq 1.8$–2.0.

Key words: dust, extinction – Galaxy: abundances – ISM: abundances – ISM: general

Online-only material: color figures

1. INTRODUCTION

Submicrometer-size grains cause attenuation of light from ultraviolet (UV) to near-infrared (NIR) wavelengths. Larger grains may form small astronomical objects. Thirty years ago, Mathis et al. (1977, hereinafter MRN) showed that dust composed of a mixture of silicate and carbonaceous grains accounts for the extinction curve from the UV to optical wavelengths, from which they derived the size distribution of grains for $a = 0.005$–$0.25\,\mu$m. Only with nine bins of the histogram, they advocated that the size distribution is consistent with the power law a^{-q} with the index q from 3.3 to 3.6.[4] This dust model is consistent with the fact that Mg, Si, and Fe are highly depleted in diffuse interstellar matter. These three elements are also major constituents of astronomical silicate with the corroborating fact that the abundance of dust needed to account for the observed extinction is on the order of magnitude of their cosmic abundance, and hence the three elements could dominantly be locked in dust.

Independently, the argument appeared that small astronomical bodies in frequent collisions would obey a power-law distribution in size (Dohnanyi 1969; Hellyer 1970; Biermann & Harwit 1980; Dorschner 1982). It was argued that the power law derived by collisional equilibrium typically has $q = 3.5$ (Dohnanyi 1969; Pan & Sari 2005), which agrees with the power favored by interstellar dust from extinction studies. For larger sizes, the distribution of small astronomical objects ($\gtrsim 1$–$10\,$km) is not in conflict with this power, while the available information is limited to derive it more accurately.

These arguments indicate that the size distribution of grains may be key to understanding the formation of grains and small astronomical objects. The size distribution of grains has been studied in the literature (e.g., Draine & Lee 1984, hereafter DL84; Kim et al. 1994; Weingartner & Draine 2001, hereafter WD01; Clayton et al. 2003b; Zubko et al. 2004). These studies stress accurately reproducing the extinction curve that is progressively more accurately measured and is extended to the NIR region, to find the detailed size distribution of grains. A significant variation has become apparent in the extinction curve depending on the line of sight (Mathis & Cardelli 1992; Clayton et al. 2000). The variation typically amounts to $R_V = 2.2$–5.5, assuming the one-parameter formula of Cardelli et al. (1989, hereafter CCM: their formula is referred to as the CCM curve), who showed that the family of extinction curves is well described by a formula with the single free parameter, $R_V = A_V/E(B - V)$, where A_V is the extinction in the V band and $E(B - V)$ is the reddening. It should be asked how the variation of the extinction curve translates to the properties of dust grains. Another important problem is determining other grain constituents beyond silicate and graphite.

Further to the shape of the extinction curve, the amounts of extinction, usually represented with $E(B - V)$ per hydrogen, gives an important constraint on the abundance of dust grains. An important question is whether the grain parameters derived from the extinction curve are consistent with those from the amount of extinction, and whether they are consistent with the elemental abundance.

It has been known that the extinction curve for the Small Magellanic Cloud (SMC) is markedly different from that for the Milky Way (MW) in that it lacks the feature at 2175 Å and it shows a significantly steeper rise to the far-UV side beyond 2000 Å. What would cause this difference is the problem to be

---

[4] For reference we attempt to fit the size distribution derived by MRN (five data points for silicate, and six for graphite) by the power law: it results in $q = 3.8 \pm 0.7$ for graphite and $q = 3.5 \pm 0.6$ for silicate, where the error stands for the dispersion.

Table 1
Interstellar Extinction Data for the Milky Way

Reference Wavelength		$1/\lambda$	$(A_\lambda/A_V)_{obs}$	
(μm)		(μm^{-1})	Lower	Upper
0.125	(far-UV rise)	8.00	2.573	3.894
0.16	(far-UV dip)	6.25	2.167	3.003
0.2175	(UV bump)	4.60	2.712	3.625
0.36	(U band)	2.78	1.449	1.62
0.44	(B band)	2.27	1.252	1.331
0.55	(V band)	1.82	1	1
1.25	(J band)	0.80	0.211	0.278
1.65	(H band)	0.61	0.127	0.166
2.17	(K band)	0.46	0.077	0.101
Ranges from the CCM formula for NIR				
1.25	(J band)	0.80	0.267	0.299
1.65	(H band)	0.61	0.171	0.191
2.17	(K band)	0.46	0.110	0.123

Notes. The allowed ranges of the interstellar extinction $(A_\lambda/A_V)_{obs}$ at the reference wavelengths constructed from the data of extinction curves of FM07. The ranges of the NIR extinction from the CCM formula is for $R_V = 2.75$–3.60. In optical regions, the ranges virtually agree with the 1σ ranges of FM07.

resolved. The SMC-type extinction curve is also indicated for interstellar clouds such as Mg II absorbers (York et al. 2006); it is shown that the majority, typically $\sim$70%, of the cloud obeys the SMC-type extinction law.

In this paper, we revisit gross but generic features of dust grains using the modern data of extinction curves from 1150 Å to 2.2 μm derived for the MW and, in the other extreme, the SMC, along with modern optical data of the relevant dielectric material. We examine whether some departure from power-law size distributions, other than cutoffs in the size, is compelling in reproducing the observed extinction curve. We are also interested in how dust in the SMC should differ from that in the MW in its properties. Furthermore, we would like to see whether the graphite–silicate model is unique and what is the possible range of dust to hydrogen mass ratio. We assume spherical grains and their size distribution obeys a power law allowing for a truncation at some maximum size. The power-law distribution, at least, can be understood with simple physics for the evolution of grains. We do not treat polarization and infrared emission from dust since either requires knowledge other than the property of dust grains and so, in turn, requires extra assumptions that would introduce further uncertainties.

In Section 2, we review the data of extinction curves used in the present study, and we note a problem in the average NIR extinction curve. After defining the model of interstellar dust used in this paper in Section 3, we search, in Section 4, for the dust model that could reproduce the observation, present parameters of the model and ask various possibilities of the favorable composition of grain species from the extinction data for the MW. We carry out a similar analysis for SMC dust in Section 5. Section 6 gives a summary of this study with discussion.

2. EXTINCTION CURVES

2.1. Milky Way Extinction

We take the extinction curves derived from UV to NIR for the 328 stars in Fitzpatrick & Massa (2007, hereafter FM07) with the aid of stellar atmosphere, replacing the traditional method using reddened-comparison pairs of stars. The extinction curve
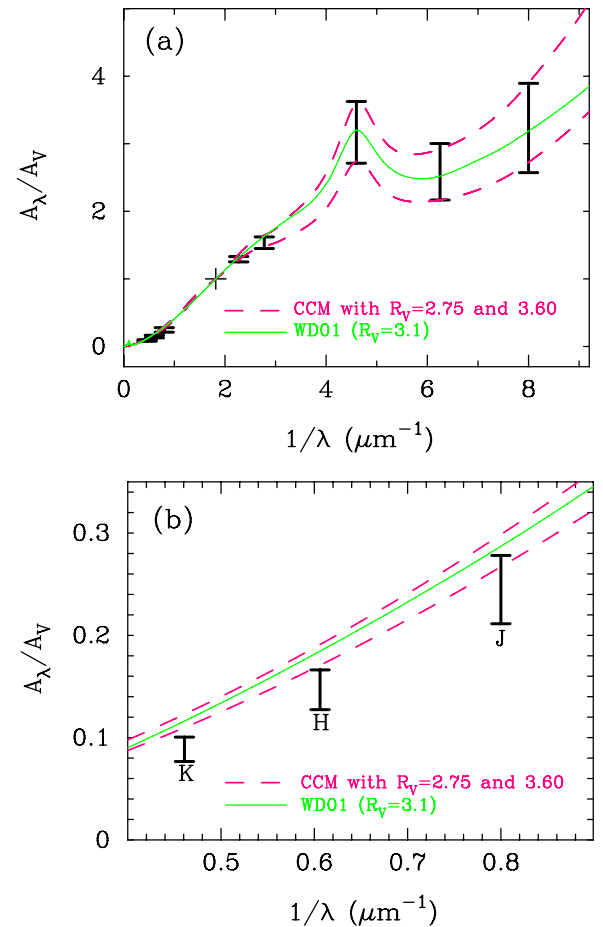

Figure 1. (a) Interstellar extinction curves from the 328 stars in the Milky Way from FM07. Our 1σ (thick solid bars) estimates are denoted at our reference wavelengths. The plus symbol shows the V band used as the normalization. (b) The expanded figure for the extinction in NIR. The bars are 1σ. The extinction curves of the CCM formula with $R_V = 2.75$ (the upper dashed curve in (a) and the lower dashed curve in (b)) and $R_V = 3.60$ (the lower dashed curve in (a) and the upper dashed in (b)), and the model of WD01 ($R_V = 3.1$, the solid curves) are shown.

(A color version of this figure is available in the online journal.)

ranges from 1150 Å to 2.2 μm. We are primarily interested in the global average of the extinction curves, so we consider a set of the curves at several specific reference wavelengths, at which we derive the allowed ranges of extinction. We take nine reference wavelengths in total with the V band to give the normalization. We consider wavelengths corresponding to $UBJHK$ and three wavelengths, $\lambda = 0.2175\,\mu$m, $0.16\,\mu$m, and $0.125\,\mu$m, in UV, which characterize the hump, the bottom in the UV region, and an arbitrary chosen wavelength in the rise of the Galactic extinction curve toward shorter wavelengths, respectively. The $UBVJHK$ passbands are those FM07 used to derive the extinction curve in the optical and NIR regions from the observation (they have not used R and I). We take the 1σ allowed ranges corresponding to 68% (224 curves) of the 328 curves at each reference point. Our wavelength mesh is too coarse to study the 2175 Å feature, so it is considered separately. We do not treat diffuse interstellar bands which are not apparent in the FM07 extinction curve. Possible line features beyond the K band are not treated.

The 1σ ranges of A_λ/A_V are shown in Table 1 and in Figure 1: (a) for the entire wavelength range considered and (b) for NIR

in an expanded scale.[5] Figure 1(a) shows that the CCM curve with $R_V = 2.75$–3.60 and the dust-model calculation of WD01 (which gives $R_V = 3.1$) are both consistent with the data of FM07 in the optical and the UV regions. In the NIR region, however, the expanded figure, Figure 1(b), indicates that both curves are off from the FM07 data by $\approx 1\sigma$ or more. This arises from the fact that CCM adopted the NIR extinction that follows the power law $A_\lambda/A_V \propto \lambda^{-\gamma}$ with the index $\gamma = 1.61$ (Rieke & Lebofsky 1985), whereas the FM07 data are consistent with a steeper index, $\gamma = 1.84$. The steeper index (Martin & Whittet 1990) has gained more support in a recent work: for example, Fitzpatrick & Massa (2009) reported the index 1.78–2.0 and that it varies according to the line of sight (see also Fritz et al. 2011 for a summary of the recent work). The slope changes between I_C and J.

We take the FM07 data as our prime choice, while tentatively retaining the possibility that the NIR power index is moderate, as with CCM and WD01. We also consider this possibility and study the implication on the dust model. We take the range of the CCM curves with $R_V = 2.75$–3.60, which correspond to 1σ of the extinction data of FM07 in the UV and optical range, as seen in Figure 1(a). Our 1σ range adopted for NIR covers the variation of the index reported by Fitzpatrick & Massa (2009), while CCM and WD01 are beyond 1σ. The difference in the NIR slope leads to a significant difference in the conclusion concerning the model.

In addition, we consider the absolute amount of extinction, or reddening. Bohlin et al. (1978) obtained for 75 stars $N_H/E(B - V) = 5.8 \times 10^{21}$ cm^{-2} mag^{-1}, which is widely adopted in the literature, and claimed that the data for different lines of sight rarely fall beyond the lines 1.5 or 1/1.5 times the value indicated in this expression. Actually, we see in their figure (their Figure 2(b)) that about 85% of stars are located between the two lines. (Most of the deviants are toward the smaller N_H side.) The N_H value includes a 25% contribution from H_2 molecules. Unfortunately, they have not given the error or the dispersion of the fit, so we have re-fitted their data to obtain the 1σ error. We have also tried to include the recent enlarged data set compiled by Gudennavar et al. (2012). After the selection similar to that in Bohlin et al. (1978), we obtain, using 174 data,

$$N_H/E(B - V) = (5.7 \pm 1.7) \times 10^{21} \text{ cm}^{-2} \text{ mag}^{-1}, \quad (1)$$

where the error stands for the dispersion of the fit. This is in good agreement with the original Bohlin et al. (1978) result, including the size of the dispersion we re-estimated from their data (± 1.7).

2.2. Extinction in the Small Magellanic Cloud

Only a handful of sightlines are studied for the extinction curve for the SMC. Gordon et al. (2003, hereafter G03) presented the curve toward five stars, AzV 18, AzV 23, AzV

Table 2
Extinction Data in the Small Magellanic Cloud

Reference Wavelength		$1/\lambda$	$(A_\lambda/A_V)_{obs}$	
(μm)		(μm^{-1})	Lower	Upper
0.125	(far-UV rise)	8.00	4.839	6.752
0.16	(far-UV dip)	6.25	3.813	5.005
0.2175	(UV Bump)	4.60	2.772	3.946
0.36	(U band)	2.78	1.521	1.892
0.44	(B band)	2.27	1.303	1.488
0.55	(V band)	1.82	1	1
1.25	(J band)	0.80	0.108	0.324
1.65	(H band)	0.61	0.000	0.184
2.17	(K band)	0.46	0.000	0.060

214, AzV 398, and AzV 456 using the traditional reddened-comparison pair of stars. The more recent result of Cartledge et al. (2005) is consistent with G03.

As known, the bump at 2175 Å is not apparent except for the sightline toward AzV 456, which is located in a "wing" region of quiescent star formation, unlike the other four that pass through the star-forming bar of the SMC. We include the extinction curve toward AzV 456 in our consideration.

For our measure, we define, because of the paucity of data, the "1σ ranges" of the extinction to be the maximum and the minimum of the five curves at each reference wavelength. If the lower value becomes negative, it is set to zero. The ranges of extinction are given in Table 2 and plotted in Figure 2.

The recent analysis for the column density of neutral hydrogen $N_{H I}$ is by Welty et al. (2012). The abundance of H_2 molecules is estimated to be 2% of hydrogen, which is compared to 25% for the MW (Bohlin et al. 1978), giving an example of molecular formation depending on environment. Their estimate is consistent with that of Tumlinson et al. (2002),[6] $2N_{H_2}/N_H = 1^{+0.5}_{-0.2}\%$. Welty et al. (2012) gave

$$N_H/E(B - V) = 2.3^{+2.8}_{-1.3} \times 10^{22} \text{ cm}^{-2} \text{ mag}^{-1}. \quad (2)$$

This is larger than the MW value given in Equation (1) by a factor of 4.0 ± 2.4. Russell & Dopita (1992) give a summary of the elemental abundance for the SMC, which indicates that its metallicity is 5.6 times smaller than solar. We note that the abundance in SMC is poorly known. The inferred dust abundance per hydrogen of the SMC, relative to the MW, is consistent with, or somewhat less suppressed compared with, the inferred heavy element abundance.

3. DUST MODEL

With spherical particles uniformly distributed in interstellar space the total extinction, A_λ, along the line of sight l, is

$$A_\lambda = 1.086 \sum_j \int dl \int_{a_{min,j}}^{a_{max,j}} \pi a^2 Q_{\lambda,j}^{ext}(a) n_j(a) da, \quad (3)$$

where $Q_{\lambda,j}^{ext}(a)$ is the extinction efficiency defined as the ratio of the extinction cross section $\sigma_{\lambda,j}(a)$ at wavelengths λ to the geometric cross section πa^2 for grain species j and is calculated using Mie scattering with the laboratory optical data of dielectric

---

[5] If we derive the extinction for R_C and I_C from FM07 in the same manner as the other passbands, the 1σ ranges are 0.722–0.778 and 0.492–0.587, respectively. We note that these data are not directly constrained by observations. In fact, direct observational determinations for the extinction for R_C and I_C are scant. Winkler (1997) estimated it assuming the fiducial colors for the estimated types of stars. His values overlap with those from FM07 at 1σ only marginally. The extinction in the I_C band discussed in Draine (2003a) extends from -1.5 to $+2.7$ σ for $R_V = 3.1$. The range derived above may underestimate the error. We do not use the extinction for R_C and I_C as the constraint: if we would take their 1.5σ error range for FM07, all constraints discussed in this work will be unchanged.

[6] The estimate of Cartledge et al. (2005) for H_2 for some of the five stars wildly varies from 5% to 50%. We quote that the cosmic global abundance of $2N(H_2)/N(H)$ is inferred to be 0.30 (Fukugita 2011).

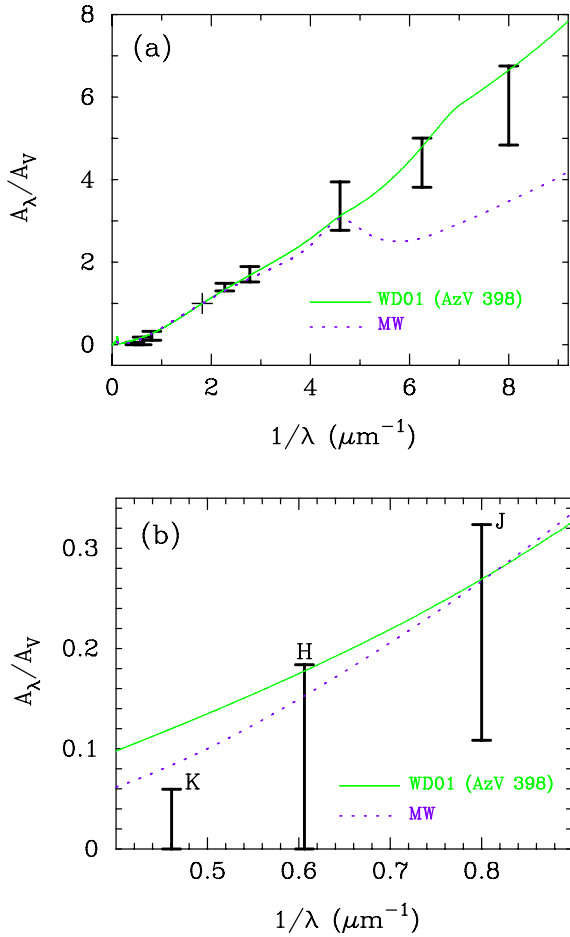**Figure 2.** (a) The extinction curves for the SMC derived from five stars by G03, with 1σ (thick solid bars) significance denoted at the reference wavelengths. The plus symbol corresponds to the V band. (b) The expanded figure for the NIR extinction. The extinction curve given by WD01 (for AzV 398) is shown by the solid line. The extinction curve for the MW, taken from Figure 3 (our model), is also added (thin dotted curves) for comparison.

(A color version of this figure is available in the online journal.)

constants: $n_j(a)da$ is the number density of the grain of species j with radius between a and $a + da$.

The "standard composition" of dust is graphite and silicate. Following DL84, we take "astronomical silicate" (we simply call it silicate unless otherwise stated) with the composition MgFeSiO$_4$. We assume the simple approximation that dust grains are bare refractory particles without substructure. For graphite, we calculate $Q_{\lambda,\mathrm{gra}}^{\mathrm{ext}}$ using the usually adopted $(1/3) - (2/3)$ approximation for the dielectric constant components perpendicular and parallel to the basal plane (e.g., DL84) to represent anisotropy.

In order to see their possible importance we also consider other refractory components and carbonaceous materials, which are likely to condense into grains, insofar as their optical properties are known. We consider 10 grain species, graphite (gra; optical data from Draine 2003b), glassy carbon (glC; Edoh 1983), amorphous carbon (amC; Zubko et al. 1996), silicon carbide (SiC; Choyke & Palik 1985), astronomical silicate (asil; Draine 2003b) of the chemical composition of olivine (Mg$_x$Fe$_{1-x}$SiO$_4$) with $x \approx 1$, forsterite (Mg$_2$SiO$_4$; Semenov et al. 2003), pure iron (Fe, Semenov et al. 2003), magnetite (Fe$_3$O$_4$; Triaud),[7] troilite (FeS; Semenov et al. 2003),

and corundum (Al$_2$O$_3$; Toon et al. 1976). We do not consider enstatite (MgSiO$_3$). One may expect that the optical property of MgSiO$_3$ is not much different from that of olivine, and its contribution may not disturb much the calculation with astronomical silicate.[8] We ignore SiO$_2$, since its Q factor is small. Inclusion of SiO$_2$ only increases the amount of Si locked in dust grains. The Ca- and Ti-bearing grains may constitute some components of dust, but they are not considered because of their small cosmic abundance.

We do not consider polycyclic aromatic hydrocarbons (PAHs) separately. The bump at 2175 Å in the Galactic extinction curve can be accounted for either with or without PAH insofar as small graphite grains (molecules with the effective radius of $\lesssim$200 Å) are included (Stecher & Donn 1965; Joblin et al. 1992; Clayton et al. 2003a).

Dust grains dominated by a single size do not give the observationally obtained extinction curve. Some distribution over the size is necessary. A typical distribution that is known to work is the power law, which we also use here

$$n_j(a) = n_{\mathrm{H}} K_j (a/a_0)^{-q_j}, \qquad (4)$$

where n_{H} is the hydrogen number density, K_j is the fraction of species j, and a_0 is a size of the normalization. We limit the range to $a_{\min,j} \leqslant a \leqslant a_{\max,j}$. We assume the same grain-size distribution independent of grain species.

We take q_j, $a_{\max,j}$, and the condensed fraction $f_{i,j}$, i.e., the fraction of element i contained in grain species j, as parameters, and find a set of the parameters that satisfy 1σ of extinction data at all nine reference wavelengths. We also study the dependence on the parameter $a_{\min,j}$, but the fit varies little insofar as this minimum size is smaller than $0.005\,\mu$m. The minimum size $a_{\min}$ affects the extinction curve in the way that increasing it diminishes the rise in the far-UV for wavelengths roughly shorter than $O(2\pi) \times a_{\min}$. With our choice of $a_{\min} = 50\,$Å it affects little the curve for $\lambda > 1150$–$1250\,$Å we consider. The increasing variation of $a_{\min}$ also affects the 2175 Å bump caused by graphite, reducing the hump, but the resulting change of the extinction curve from the decreasing variation of $a_{\min}$ from $0.005\,\mu$m to 0 is small, typically $<1/3$ the 1σ error range. The parameter $a_{\min}$ is not well determined if it is left as a free parameter, unless the extinction data of shorter wavelengths are used. Thus we fix $a_{\min}$ at $0.005\,\mu$m.[9] The change of lower cutoff affects little the determination of the other parameters, unless $q \gtrsim 4$, which is deep in the region not allowed in our study. It increases the total amount of mass, say, by 10% if $a_{\min}$ is reduced from $0.005\,\mu$m to $0.001\,\mu$m. A possible increase of the lower cutoff for graphite is considered for SMC dust separately. The extinction curve we refer to is A_λ/A_V, normalized in the V band

$$\frac{A_\lambda}{A_V} = \frac{\sum_j K_j A_{\lambda,j}}{\sum_j K_j A_{V,j}}, \qquad (5)$$

where $A_{\lambda,j}$ is the component contribution to Equation (3).

---

[7] A. Triaud, http://www.astro.uni-jena.de/Laboratory/OCDB/oxsul.html

[8] The imaginary part of the presently available refractive index of enstatite (Dorschner et al. 1995) deviates largely from that of forsterite in the UV region, while the real part differs little. The Q factor of enstatite differs little from that of forsterite. We do not treat enstatite separately in this paper.

[9] Considering a possible importance of small grains beyond the power law in the IR emission, we examined the possibility that some non-negligible amounts of grains are distributed below $a_{\min}$. The presence of such grains, say, at 0.001 or 0.005 μm, modifies most characteristically the UV slope, making it steeper at wavelengths shorter than 2000 Å and the hump at 2175 Å larger. Insofar as these extra components are less than 15% in mass, our resulting extinction curves are not changed beyond our reference errors.

We also calculate

$$\frac{E(B-V)}{N_{\rm H}} = 1.086 \sum_j K_j \int_{a_{\min,j}}^{a_{\max,j}} da (\sigma_{B,j} - \sigma_{V,j})(a/a_0)^{-q_j}.$$

(6)

The amount of reddening per hydrogen leads to the constraint on the abundance of dust that can be compared with other elemental abundance estimates. Assuming that the abundance does not vary from place to place, we take as standard for the MW the solar elemental abundance estimated by Grevesse & Sauval (1998, hereafter GS98).[10] Asplund et al. (2009), using three-dimensional (3D) calculation, claimed that the solar abundance is generally lower than that of GS98 by as much as 30%, especially for C, O, and a few others. A comparable 3D calculation (Caffau et al. 2011), however, has given an abundance that is lower than GS98 only by 10%.

The elemental abundance is generally not tightly converged among the authors. For instance, for the carbon abundance, which is of one of our major concerns, the GS98 value C/H = $(3.3 \pm 0.5) \times 10^{-4}$ may be compared with 3.62×10^{-4} of Anders & Grevesse (1989), 2.69×10^{-4} of Asplund et al. (2009), 3.16×10^{-4} of Caffau et al. (2011), $(1.9-2.9) \times 10^{-4}$ of Cardelli et al. (1996), 2.14×10^{-4} of Nieva & Przybilla (2012), 2.45×10^{-4} of Lodders (2010), and so forth. The iron abundance, for which GS98 give $\log(\text{Fe}/\text{H}) + 12 = 7.50 \pm 0.05$, too, varies between 7.45 and 7.66. Keeping these uncertainties in mind, we take as our default GS98, which leads to a satisfactory solar structure.

For the SMC we take the composition given by Russell & Dopita (1992), with which the total metallicity is 1/5.6 times solar. The abundance of refractory elements, Mg, Si, and Fe, is smaller than their MW values by factors 1/3.3–1/4.6. The abundance of O and C in the SMC seems more strongly depressed by 1/(6.2–6.3) times, compared with the solar abundance. Taken literally, this leads to the significant result that the ratio of carbonaceous material to silicate in the SMC is 50% lower than the corresponding value for the MW. We must remember, however, that the elemental abundance for SMC is probably more uncertain than for MW.

4. RESULTS FOR MW DUST

4.1. Single Grain Species

We first study the extinction curve with a single grain species. We consider the allowed region in the q and $a_{\max}$ plane, with which the dust model satisfies the 1σ ranges of the FM07 extinction curve. We find that there is no overlap among the three regions derived from the UV group (0.125 μm, 0.16 μm, and 0.2175 μm), the UBV group, and the NIR group (J, H, and K) for any species of grains we considered. The regions required for the UV and UBV groups are always disjoint. It often happens that no consistent parameters exist for J, H, and K, the NIR passbands alone. We cannot make a dust model which explains the extinction curve over the wide range of wavelength with only a single grain species. For instance, astronomical silicate gives too steep a rise in the far-UV if $a_{\max}$ is chosen to account for the optical extinction curve, and the predicted NIR extinction is too small by a factor of 3–4. We expect that these problems are offset by introducing carbonaceous grains, which give a milder

Table 3
Extinction Data A_λ/A_V for the Milky Way

Wavelength		A_λ/A_V		
(μm)		Our Work	CCM ($R_V = 3.1$)	WD01 ($R_V = 3.1$)
0.3531	(u)	1.633	1.584	1.660
0.365	(U)	1.583	1.557	1.608
0.44	(B)	1.306	1.325	1.318
0.4627	(g)	1.232	1.243	1.246
0.55	(V)	1.000	1.000	1.000
0.6140	(r)	0.866	0.884	0.859
0.66	(R_c)	0.785	0.812	0.774
0.7467	(i)	0.660	0.678	0.646
0.81	(I_c)	0.582	0.583	0.571
0.8887	(z)	0.498	0.489	0.493
1.25	(J)	0.267	0.282	0.287
1.65	(H)	0.153	0.180	0.185
2.17	(K)	0.0836	0.116	0.117
3.35	(WISE1)	0.0348	0.0577	0.0513
3.55	(IRAC1)	0.0313	0.0525	0.0463
4.44	(IRAC2)	0.0213	0.0367	0.0297
4.60	(WISE2)	0.0201	0.0346	0.0280

Note. Our model extinction is compared with those of CCM and WD01.

rise in the far-UV and have a larger scattering efficiency in the NIR bands, and we suppose that the mixture of these two species would give the correct extinction curve.

4.2. Graphite–Silicate Dust Model

The two-component dust model, consisting of graphite and astronomical silicate, has been widely taken for interstellar dust since MRN. Mg, Si, and Fe are similar in the cosmic number abundance (within 20%). If we assume that Si is all condensed into astronomical silicate, $f_{\text{Si,asil}} = 1$, then $f_{\text{Mg,asil}} = 0.93$ and $f_{\text{Fe,asil}} = 1$, if Fe:Mg = 1:1 (see Draine 2003a) with the GS98 abundance. Here, iron is slightly (10%) deficient and extra Si and Mg may condense into forsterite. Oxygen locked in silicate is $f_{\text{O,asil}} = 0.26$. Carbon is also depleted in interstellar matter. Following Sofia et al. (2011), it is approximately 60%–70%, i.e.,

$$f_{\text{C,gra}} = 0.6 - 0.7$$

(7)

if all condensed carbon is in graphite. This is higher than their earlier estimate, 30%–40%.[11] The depletion given by Cardelli et al. (1996) is also consistent with Equation (7) if the GS98 abundance is adopted.

The model attains good fits from far-UV to NIR within 1σ of the data with

$$q = 3.5 \pm 0.2 \text{ and } a_{\max} = 0.24^{+0.10}_{-0.05}.$$

(8)

The range of $f_{\text{C,gra}}/f_{\text{Fe,asil}}$ is 0.25–2.23, allowing for $f_{\text{Fe,asil}} < 1$. Figure 3 presents examples of the resulting extinction curve from our model at the central values of Equation (8) with $f_{\text{C,gra}}/f_{\text{Fe,asil}} = 0.7$. We give in Table 3 numerical values of A_λ/A_V for selected wavelengths (and compare them with the models of WD01 and CCM). We underline the discrepancy between our model and WD01 (and also CCM) increasing from the J band longward. It becomes 30% for the K band. We draw several curves in addition that are somewhat away from the best-fit value (say, about 1.5σ of the observation) to indicate how the

---

[10] We remark that GS98 agree with the earlier table of Anders & Grevesse (1989) up to oxygen, for which the GS98 value is lower by 0.1 dex.

[11] Sofia et al. (2004) used only weak absorption lines of carbon, while their updated analysis (2011) includes strong absorption lines.
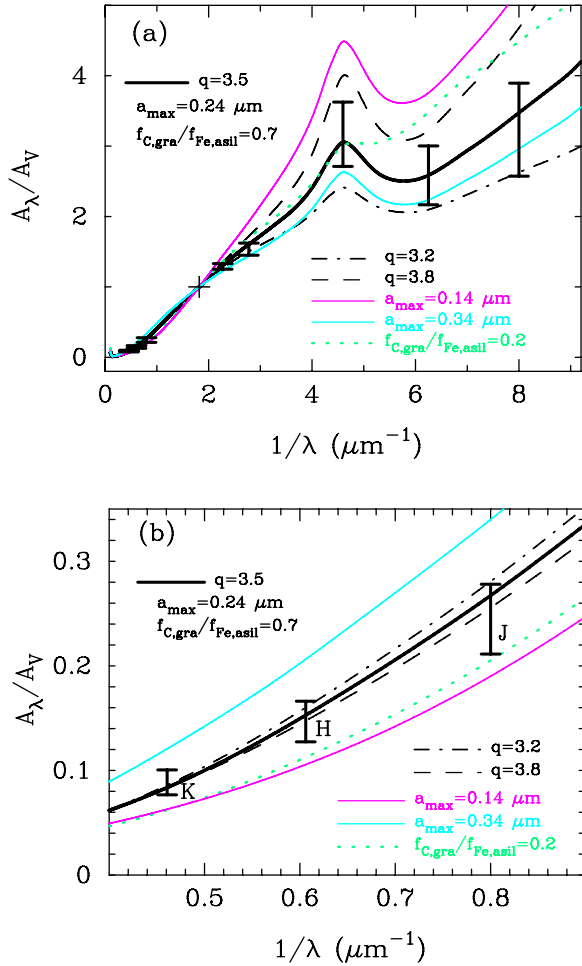
Figure 3. (a) Typical extinction curves from the graphite–silicate models, and (b) the expanded figure of (a) for NIR wavelengths. The error bars stand for the observed 1σ ranges. The thick solid curve is with $q = 3.5$, $a_{max} = 0.24\,\mu m$, and $f_{C,gra}/f_{Fe,asil} = 0.7$, taken as our fiducial. The other curves denoted by thin curves are examples where one of the three parameters is shifted to demonstrate the response to the parameter. The legend shows the parameters when changed from the fiducial choice.

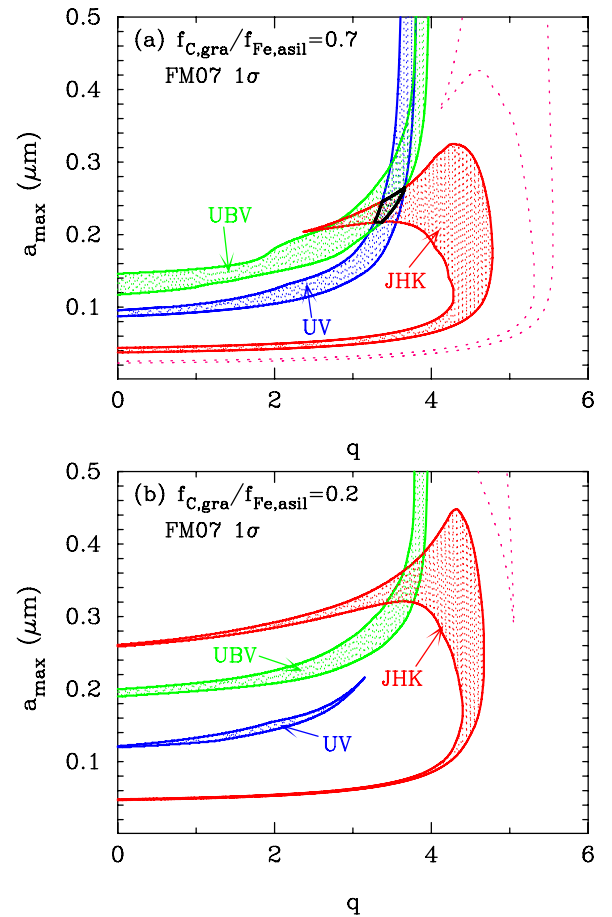(A color version of this figure is available in the online journal.)

Figure 4. Allowed parameter regions for graphite–silicate models in q and a_{max} plane for the 1σ range in the UV group (blue), the UBV group (green), and the NIR (*JHK*) group (red). We take $f_{C,gra}/f_{Fe,asil} = 0.7$ in (a) and 0.2 in (b), the latter of which is a model out of 1σ. Thin dotted curves show the parameters for the 1σ range in the NIR (*JHK*) group when the NIR wavelength dependent power is $\gamma = 1.6$ as with CCM or WD01.

(A color version of this figure is available in the online journal.)

curve shifts with the variation of q, a_{max}, and $f_{C,gra}/f_{Fe,asil}$. The mass density ratio of graphite to astronomical silicate is given by $\rho_{gra}/\rho_{asil} = 0.73 f_{C,gra}/f_{Fe,asil}$. We note that our curve is in close match with the WD01 curve ($R_V = 3.1$) from the U to I_C passbands.[12] A significant departure starts from the J band longward. The role of graphite is, in addition to producing the 2175 Å bump, to increase the extinction in NIR, which is too small with silicate alone when normalized in the optical region. Graphite makes the rise in the far-UV more moderate.

In Figure 4, we show in $q - a_{max}$ plane the region where the model gives the 1σ ranges of the extinction for the choices of $f_{C,gra}/f_{Fe,asil} = 0.7$ and 0.2. The overlapping region is seen for UV, UBV, and NIR for $f_{C,gra}/f_{Fe,asil} = 0.7$, validating the graphite–silicate model. Such allowed regions disappear for $f_{C,gra}/f_{Fe,asil} \leqslant 0.25$.

Figure 5 shows the abundances of carbon and silicon in grains necessary to account for the extinction curve relative

to hydrogen. The allowed region extends in a belt, running from bottom left to top right, representing $f_{C,gra}/f_{Fe,asil} = $ const. We also indicate the region allowed from $E(B - V)/N_H$, which is located near the center of the belt (lightly shaded). This leads to the elemental abundance carried by dust grains,

$$\log (C/H) + 12 = 8.4 \pm 0.3 \text{ and } \log (Si/H) + 12 = 7.6 \pm 0.4.$$
(9)

We also indicate the abundance of GS98 for Si (7.55; horizontal dashed line) and C (8.52; vertical horizontal line) with the neighboring shade showing various abundance estimates.

The abundances resulted from the interstellar extinction are consistent with other estimates. If we take the GS98 value for the total abundance of C and Si including the gas phase, the figure, showing $\log (C/H) + 12 \geqslant 8.27$, means

$$f_{C,gra} \geqslant 0.56,$$
(10)

for $f_{Si,grain} = 1$ assumed. This carbon fraction in graphite is consistent with the depletion estimated for interstellar matter quoted in Equation (7).[13]

---

[12] Our curve lies at the 1σ edges if we take the R_C and I_C data constructed from the FM07 curves. The constraints on the $q - A_{max}$ plane are unchanged if we take the 1.5 σ of R_C and I_C. Note that we do not use the R_C and I_C extinction data of FM07, which are not observationally constrained.

[13] The carbon abundance required from the extinction is still consistent with the lower abundance of Asplund et al. (2009), but then the depletion must be as high as >80%.
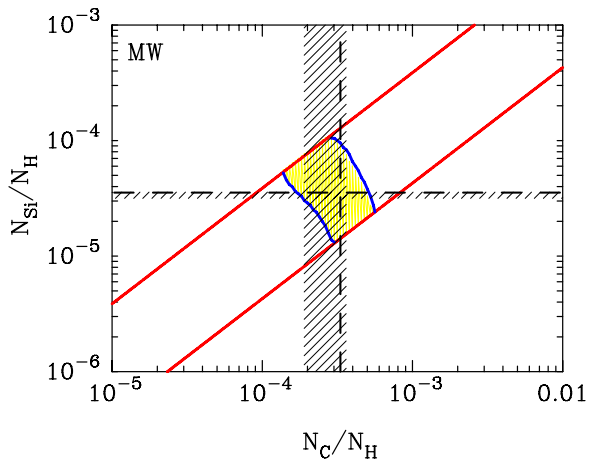
Figure 5. Abundance of C and Si in dust grains relative to hydrogen for the MW to satisfy the 1σ range of the extinction curve. The range within the oblique belt is allowed from the extinction curve, and the further restricted range in the middle is from $E(B - V)/N_H$. The two horizontal and vertical dashed lines show the total abundance of Si and C from GS98, with the shaded regions corresponding to the range of various estimates.
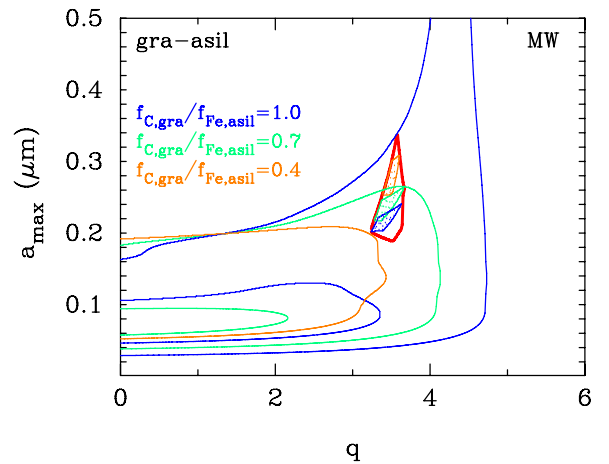

Figure 6. Allowed regions of q and a_{max} with which the model satisfies the 1σ ranges of the observed extinction for the MW, marginalized over the graphite-to-silicate ratios $f_{C,gra}/f_{Fe,asil} \geqslant 0.25$. The three contours inlaid in the allowed region indicate those with $f_{C,gra}/f_{Fe,asil} = 1.0$, 0.7, and 0.4. The constraints from the reddening $E(B - V)/N_H$ are shown for $f_{C,gra} = 0.4$, 0.7, and 1.0 (with $f_{Fe,asil} = 1.0$), drawn by thin (brown, green, and blue) contours.

A similar consideration is made for the 1σ ranges from the CCM formula, where the NIR extinction takes a smaller power index of the wavelength dependence. The range of q and a_{max} required for the NIR extinction curve is shown in Figure 4 with dotted curves (those for UV and UBV remain unchanged). We see that the region allowed simultaneously for the three groups of color bands does not exist. The region for NIR is always disjoint from those for UBV and UV. No graphite–silicate model is consistent with the observed extinction, if the NIR extinction power is $\approx \lambda^{-1.6}$, for grains with the power-law size distribution.

The steeper wavelength dependence for the NIR power thus looks more easily accommodated from the model point of view. We remark that WD01 tweaked significantly the grain-size distribution from the power law, separately for graphite and silicate, adding different components so that the graphite–silicate model becomes consistent with the CCM-like extinction. This is also true for the size distributions obtained by other authors (listed earlier) when the CCM-like extinction is reproduced with the graphite–silicate model. We note that the solution of WD01 takes the Si, Mg, and Fe cosmic abundance larger by 30%–50% than the GS98 cosmic value.

We note that the allowed regions in Figure 4 above stand for the ranges consistent with the variation of dust properties along lines of sight in the MW. They are well converged to the narrow regions of q and a_{max} indicated in Equation (8), despite an apparently significant variation of extinction curves. The size of grains is similar; only a small variation of the size parameter could cause the difference in the extinction curve.

We summarize in Figure 6 the region allowed for a_{max} and q, marginalizing over the ratio of condensed fractions of graphite to silicate for $f_{C,gra}/f_{Fe,asil} \geqslant 0.25$. The curves are inlaid for $f_{C,gra}/f_{Fe,asil} = 0.4$, 0.7, and 1. The 1σ allowed range is realized with $3.2 \leqslant q \leqslant 3.7$ and $0.19\,\mu m \leqslant a_{max} \leqslant 0.34\,\mu m$. With increasing $f_{C,gra}$, a_{max} becomes smaller. The other set of curves is the constraint from $E(B - V)/N_H$ for $f_{C,gra} = 0.4$, 0.7, and 1 with $f_{Fe,asil} = 1$. Overlaps are seen between the two curves for $f_{C,gra}/f_{Fe,asil} = 0.7$ and 1, but not for 0.4.

For our model that satisfies the 1σ constraints of both extinction curve and the $E(B - V)$ size we have the mass density of dust relative to that of the hydrogen gas, $\rho_{dust}/\rho_H = 1/(122^{+48}_{-75})$. The allowed range would be tightly constrained if

the abundance is fixed to GS98 and $f_{Fe,asil} = 1$ is assumed

$$\rho_{dust}/\rho_H = 1/\left(122^{+9}_{-16}\right). \qquad (11)$$

The mass extinction constant $K_{ext,\lambda} = A_\lambda/\Sigma_{dust}$ for the V band is

$$K_{ext,V} = (3.7 \pm 0.5) \times 10^4 \text{ mag cm}^2 \text{ g}^{-1}, \qquad (12)$$

which is compared to 2.8×10^4 mag cm^2 g^{-1} of WD01. (If the abundance constraints are removed, Equation (12) becomes $(3.6 \pm 1.0) \times 10^4$ mag cm^2 g^{-1}.) The ratio of the mass density of graphite to silicate is $\rho_{gra}/\rho_{asil} = 0.51^{+0.22}_{-0.10}$, or in terms of the number of C and Fe atoms in grains, $N_C/N_{Fe} = 7.3^{+3.2}_{-1.4}$, corresponding to Equation (11).

4.3. Inclusion of Other Carbonaceous Grains

Various populations of carbonaceous grains may constitute cosmic dust in addition to graphite. We explore the possible significance of other carbonaceous species, such as glassy carbon or amorphous carbon. We find, however, that the two-component dust model, composed of glassy or amorphous carbon and astronomical silicate, does not give the extinction curve that lies in the 1σ ranges of observation for any $f_{C,glC}/f_{Fe,asil}$ and $f_{C,amC}/f_{Fe,asil}$ ratios. These carbonaceous grains do not give the proper UV bump at 2175 Å. Glassy carbon shows a broad hump at around 2000 Å, and amorphous carbon only has a broad maximum at around 2000 Å. We consider in the following the model in which graphite is partly replaced with glassy or amorphous carbon.

Figure 7 shows a few example extinction curves for three-component models, compared with our fiducial graphite–silicate model, with $q = 3.5$ and $a_{max} = 0.24\,\mu m$, fixed at the same parameters. While some of the resulting curves displayed do not satisfy the 1σ range, as we replace graphite with these components excessively and/or we do not tweak the other parameters, we maintain this set of parameters to see how the extinction curve is modified with the inclusion of other carbonaceous material.

Varying the (q, a_{max}) parameters, we examine to what extent graphite can be replaced with glassy or amorphous carbon in the graphite–silicate model to maintain the extinction curve within the 1σ range. Figure 8 presents the maximum fraction of C
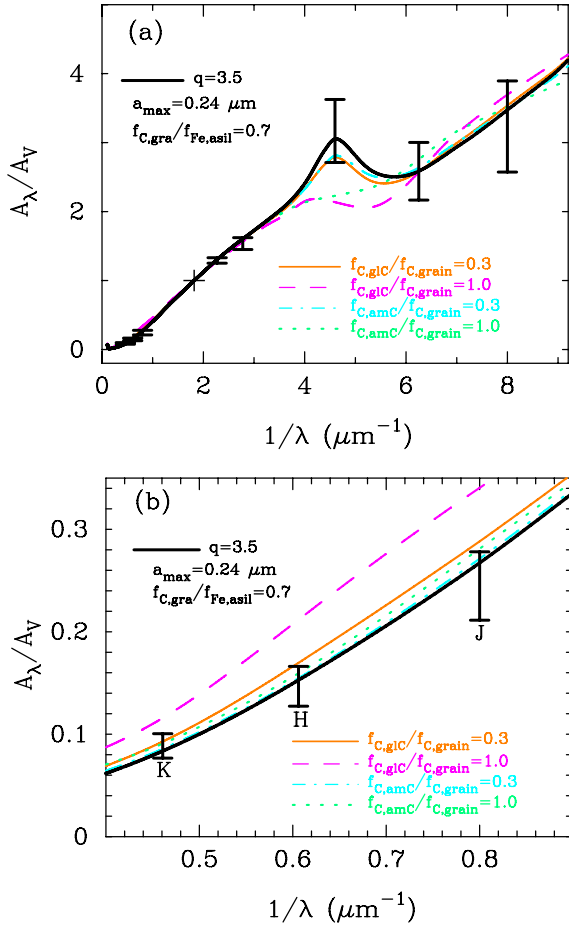
7

Figure 7. (a) Extinction curves from the graphite–glassy (or amorphous) carbon–silicate models with $q = 3.5$ and $a_{max} = 0.24\,\mu$m, and (b) the expanded figure of (a) for NIR, as compared with our fiducial graphite–silicate model (thick black curve). $f_{C,grain}/f_{Fe,asil} = 0.7$ is taken for all cases. The 1σ ranges from the observed extinction curves in FM07 are indicated with error bars.
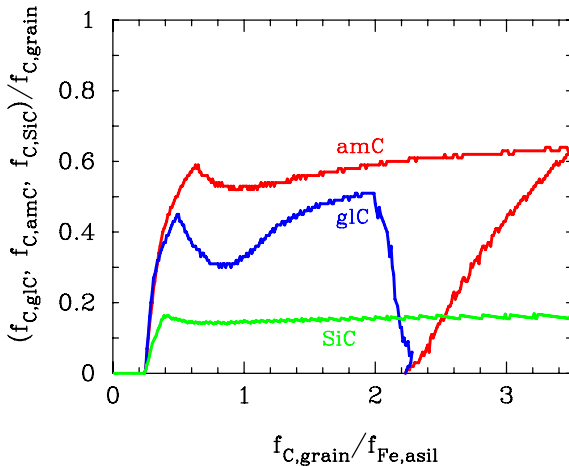

Figure 8. Allowed fractions of C atoms in the glassy phase ($f_{C,glC}/f_{C,grain}$, blue), amorphous phase ($f_{C,amC}/f_{C,grain}$, red), and silicon carbide ($f_{C,SiC}/f_{C,grain}$, green). The abscissa is $f_{C,grain}/f_{Fe,asil}$, where $f_{C,grain} = f_{C,glC} + f_{C,gra}$ or $f_{C,grain} = f_{C,amC} + f_{C,gra}$ or $f_{C,grain} = f_{C,SiC} + f_{C,gra}$. The ordinate is the maximally allowed fraction of the individual component.

atoms in glassy ($f_{C,glC}$) or amorphous carbon ($f_{C,amC}$) relative to the entire condensed component of carbon $f_{C,grain}$ against $f_{C,grain}/f_{Fe,asil}$, where $f_{C,grain} = f_{C,glC} + f_{C,gra}$ or $f_{C,grain} = f_{C,amC} + f_{C,gra}$. We see that up to $\approx$30%–40% or $\approx$50%–60% of carbon in grains can be in the glassy or amorphous phase,

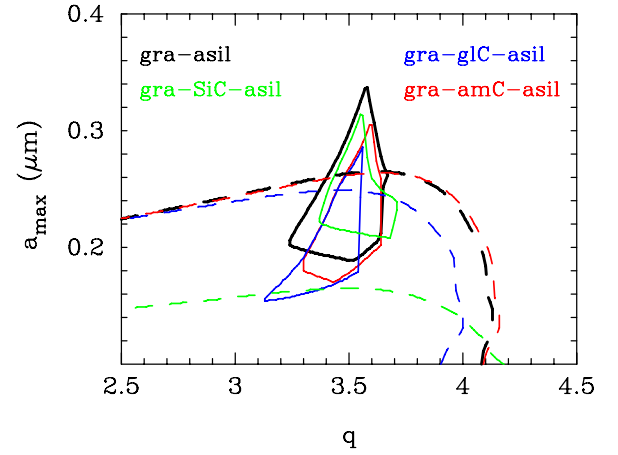**Figure 9.** Allowed regions of q and a_{max} with which the model satisfies the 1σ extinction ranges for the MW when glassy carbon, amorphous carbon, or silicon carbide is included in the graphite–silicate model. The parameters are marginalized over $f_{C,grain}/f_{Fe,asil}$. The regions that satisfy the observed size of reddening $E(B - V)$ are also shown (dashed curves) for $f_{C,grain} = 0.7$ and $f_{Fe,asil} = 1.0$. The blue, red, and green lines are, respectively, for the cases where glassy carbon, amorphous carbon, and SiC are added to the graphite–silicate model, which is represented by the black curves for comparison. For the $E(B-V)/N_H$ constraint, it is taken that $f_{C,glC}/f_{C,grain} = 0.3$, $f_{C,amC}/f_{C,grain} = 0.3$, and $f_{C,SiC}/f_{C,grain} = 0.1$.

respectively. In other words, more than 60%–70% or 40%–50% of C atoms must be in graphite. With this inclusion, the parameters (q, a_{max}) are shifted only a little; see Figure 9. Our representative parameters $q = 3.5$ and $a_{max} = 0.24\,\mu$m still remain to be in the allowed solution.

SiC is another candidate material that can be in dust grains. The upper limit of carbon contained in SiC is approximately 15% to reproduce the extinction curve (see Figure 8). This implies that SiC could be a major component of Si-bearing grains. The abundance of SiC, however, has been tightly limited to $<$4% of silicon from the lack of $11.3\,\mu$m feature in the extinction curve (Whittet et al. 1990; Chiar & Tielens 2006). The SiC component can be neglected in the discussion of the extinction curve.

In conclusion, the inclusion of amorphous or glassy carbon has little effect on the agreement of the graphite–silicate model with observations. The inclusion, however, does not make the overlap of the two constraints easier. The dust to gas ratio is unchanged from the graphite–silicate model. With SiC the overlap of the two constraints becomes marginal, and the dust to gas ratio becomes $\rho_{dust}/\rho_H = 1/(122^{+60}_{-16})$.

4.4. The 2175 Å Feature

With small graphite, the feature at 2175 Å is generated. It is known that this feature is observationally fit well with the Drude formula, including a smooth background,

$$\frac{A_\lambda}{A_V} = \frac{1}{R_V}\left[c_0 + c_1\lambda^{-1} + \frac{c_2}{\gamma_1^2 + \lambda^2\left(\lambda^{-2} - \lambda_0^{-2}\right)^2}\right] + 1. \quad (13)$$

In Figure 10, we give the central wavelength $x_0 = \lambda_0^{-1}$ and the width of the profile γ_1 for 328 extinction curves of FM07, which are summarized as

$$\lambda_0 = 2178 \pm 10\ \text{Å}, \quad \gamma_1 = 0.95 \pm 0.1\ \mu\text{m}^{-1}. \quad (14)$$

We fit the feature from our graphite–silicate model, which reads

$$\lambda_0 = 2186 \pm 12\ \text{Å}, \quad \gamma_1 = 1.21 \pm 0.08\ \mu\text{m}^{-1}, \quad (15)$$
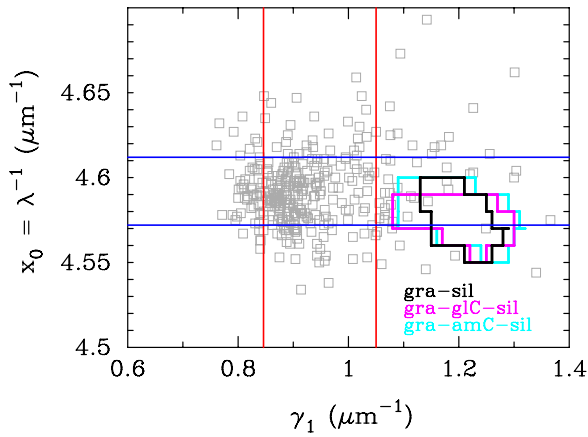
Figure 10. Central wavelength and the width parameter that describe the 2175 Å feature of the MW extinction. The observed data from FM07 (squares) are compared to our model with the parameters that gives a good fit (within 1σ of the full extinction curve) to the global extinction curve. The horizontal and vertical lines indicate 1σ of the data.

(A color version of this figure is available in the online journal.)

indicating that the model width is broader by 30% (see also Draine & Malhotra 1993), while the central wavelength agrees with the observation. We also show models with amorphous or glassy carbon included with its fraction and size parameters in the range allowed from the entire extinction curve. Their inclusions make the width slightly ($\approx$10%) smaller, but not sufficient to give the observed width. This seems to be a problem intrinsic to the optical data we adopted for graphite. More detailed treatments may be needed for small graphite or PAH.

4.5. Inclusion of Fe, Fe₃O₄, FeS, and Al₂O₃

We consider how much iron can be incorporated in generic iron-bearing grains rather than in astronomical silicate. Figure 11 shows the extinction curve for the model with our typical parameters $q = 3.5$ and $a_{max} = 0.24\,\mu m$. Figure 12 exhibits the upper limits of the fraction of Fe in the metallic phase ($f_{Fe,Fe}$, solid line) and in magnetite, Fe₃O₄ (f_{Fe,Fe_3O_4}, dashed line), for the model that satisfies the 1σ ranges of the extinction curve. The rest of the Fe atoms in interstellar space are assumed to be condensed in astronomical silicate, i.e., $f_{Fe,grain} = f_{Fe,Fe} + f_{Fe,asil} = 1$ or $f_{Fe,grain} = f_{Fe,Fe_3O_4} + f_{Fe,asil} = 1$, and Mg not included in astronomical silicate is assumed to be in forsterite, so that $\sum_{j=grain} f_{Mg,j} = 1$. Here, the abscissa is chosen to be the C/Fe ratio of the condensation.

There are parameters ($f_{C,gra}/f_{Fe,grain} = 0.15$–$1.43$) for which Fe may stay entirely in the metallic phase rather than in astronomical silicate, yet the model gives the correct extinction curve. A similar parameter range, however, is very small with the Fe₃O₄–graphite–forsterite model. Practically, the maximum allowed abundance of Fe₃O₄ is about 80%. The NIR extinction of Fe₃O₄ is large by more than a factor of two compared with the observed extinction, whereas Fe grains give the extinction in NIR only by $\approx$30% larger, and, therefore, the abundance of magnetite is limited from the extinction curve in NIR more strongly. The 1σ allowed (q, a_{max}) parameters with these models are shown in Figure 13.

The combination of metallic Fe and forsterite works virtually in the same way as astronomical silicate, which means that the Mg/Fe ratio in astronomical silicate is arbitrary. The situation is somewhat different if iron is in magnetite. The inclusion of Fe₃O₄ disturbs the allowed range in the (q, a_{max}) plane by an
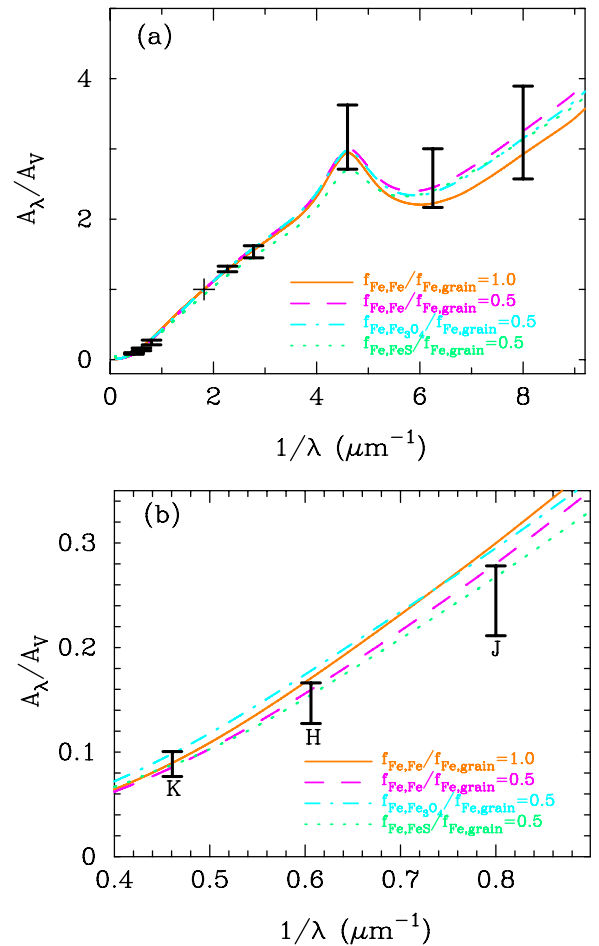

Figure 11. (a) Extinction curves for the graphite–silicate model where iron-bearing silicate is replaced with metallic Fe, Fe₃O₄, or FeS, while the corresponding silicate portions are replaced with forsterite (Mg₂SiO₄). We take the grain-size parameters, $q = 3.5$ and $a_{max} = 0.24\,\mu m$. (b) The expanded figure for the NIR. We take $f_{C,grain}/f_{Fe,grain} = 0.7$.

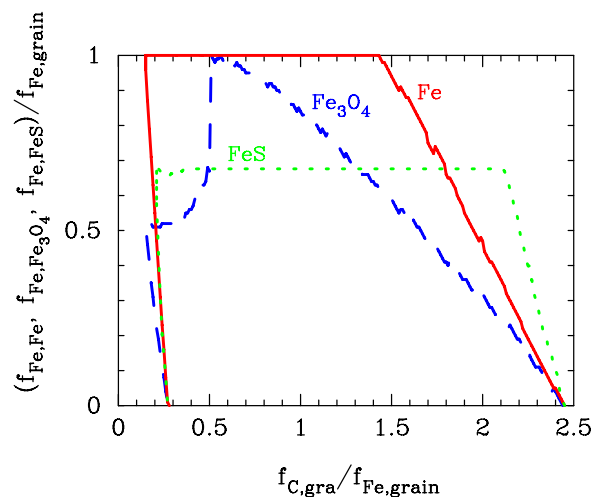(A color version of this figure is available in the online journal.)

Figure 12. Maximum fractions of Fe atoms allowed in the metallic ($f_{Fe,Fe}/f_{Fe,grain}$, red solid) or the magnetite phase, Fe₃O₄ ($f_{Fe,Fe_3O_4}/f_{Fe,grain}$, blue dashed), with which the model satisfies the 1σ extinction range for the MW. The maximum fraction is also drawn for FeS ($f_{Fe,FeS}/f_{Fe,grain}$, green dotted). The abscissa is $f_{C,gra}/f_{Fe,grain}$, where $f_{Fe,grain} = f_{Fe,Fe} + f_{Fe,asil}$, $f_{Fe,grain} = f_{Fe,Fe_3O_4} + f_{Fe,asil}$, or $f_{Fe,grain} = f_{Fe,FeS} + f_{Fe,asil}$, and the ordinate is the fraction of each species added to the model.

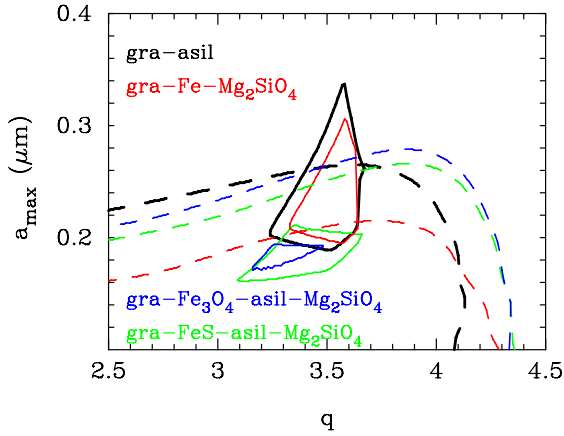(A color version of this figure is available in the online journal.)

Figure 13. Allowed regions of q and a_{max} with which the model satisfies the 1σ extinction ranges for the MW, marginalized over $f_{C,gra}/f_{Fe,grain}$. For the $E(B - V)/N_H$ constraint, we take $f_{C,gra} = 0.7$ and $f_{Fe,grain} = 1.0$. The blue, red, and green curves are, respectively, for the inclusion of metallic Fe, magnetite ($f_{Fe_3O_4}/f_{Fe,grain} = 0.8$), and FeS ($f_{FeS}/f_{Fe,grain} = 0.68$). The black curve is our fiducial graphite–silicate model.

(A color version of this figure is available in the online journal.)

appreciable amount, making a_{max} smaller by 20%. Nevertheless, we see that the overlap of the two constraints is maintained.

The cosmic abundance of sulfur is about 0.7 times that of Fe. We consider the case where all S is in troilite, FeS. The rest of Fe is in astronomical silicate and the rest of Mg is in forsterite. Troilite also gives large NIR extinction almost as much as magnetite, but the maximal amount of FeS is allowed because of the smaller cosmic abundance of sulfur. This case satisfies the 1σ constraint with a_{max} somewhat smaller than the graphite–silicate model, as seen in Figure 13.

In conclusion, iron can be in a variety of grain species, including olivine, metallic phase, Fe$_3$O$_4$, or FeS without disturbing the extinction curve. The only condition is that Fe is not predominantly in magnetite, which produces too large an NIR extinction. The grain-size parameters are nearly the same for all cases, up to the result that the maximum size cutoff becomes 20%–30% smaller if Fe$_3$O$_4$ or FeS is the major component. All iron atoms need not necessarily be locked in astronomical silicate, and the ratio of Fe:Mg in astronomical silicate is arbitrary. Allowing for the inclusion of a variety of iron material, the mass density of dust differs little from the graphite–silicate model.

We can ignore the contribution from corundum (Al$_2$O$_3$). In addition to the small abundance of Al (1/13 of Mg), the Q factor for corundum is small (Toon et al. 1976). Even if all Al atoms are locked in corundum, they contribute little to modifying the extinction curve.

Table 4 summarizes our result for most grain species we considered in the present work. Limiting ourselves to at most four grain species, we consider what combination of species would give the extinction curve consistent with the observation at 1σ. Some of them were already discussed in the text above. We take the species as valid when its fraction is more than 10%. We here note one particular case that can reproduce the extinction law of CCM: it is the combination of graphite, astronomical silicate, and magnetite. This is due to the particularly large Q factor of magnetite in the NIR, which is excluded if we take FM07.

5. DUST IN THE SMC

Figure 14 shows examples of the model extinction curve for the SMC with $q = 3.5$ and $a_{max} = 0.24\,\mu m$ for $f_{C,gra}/f_{Fe,asil} =$
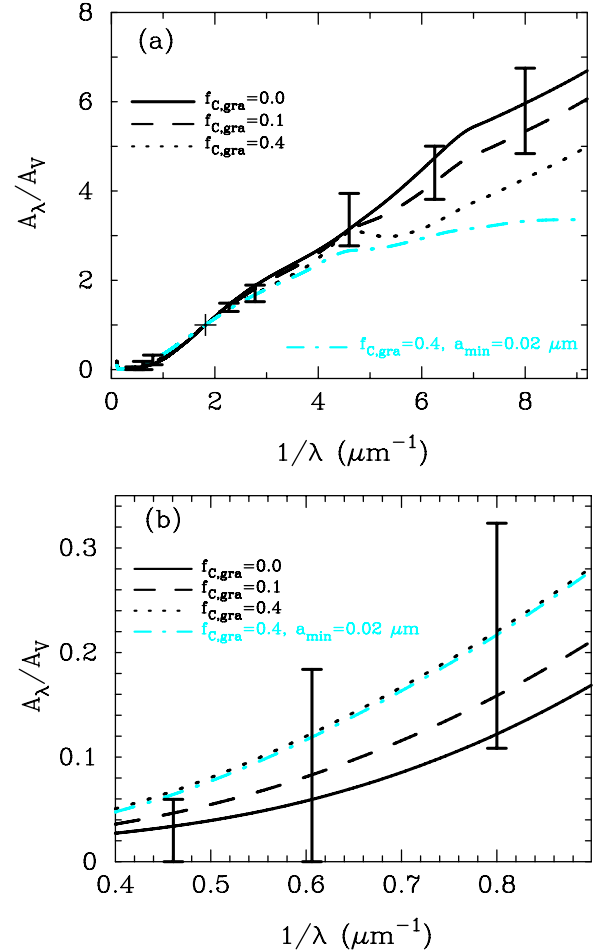

Figure 14. (a) Extinction curves for the SMC from the graphite–silicate dust models with $q = 3.5$ and $a_{max} = 0.24\,\mu m$, and (b) the expanded figure of (a) for the NIR. The solid, dashed, and dotted curves are, respectively, for $f_{C,gra}/f_{Fe,asil} = 0$, 0.1, and 0.4 with $a_{min} = 0.005\,\mu m$ fixed as our fiducial choice. The dot-dashed line is with the minimum cutoff increased to $a_{min} = 0.02\,\mu m$, while $f_{C,gra}/f_{Fe,asil} = 0.4$. The error bars span the maximum and minimum (taken as "1σ") of the observed SMC extinction curves of G03.

(A color version of this figure is available in the online journal.)

Table 4
Allowed Grain Species

Dust Grains	FM07 1σ	CCM 1σ
(1) Graphite–astronomical silicate	Yes	No
(2) Glassy carbon–astronomical silicate	No	No
(3) Amorphous carbon–astronomical silicate	No	No
(4) Graphite–glassy carbon–astronomical silicate	Yes	No
(5) Graphite–amorphous carbon–astronomical silicate	Yes	No
(6) Graphite–SiC–astronomical silicate	Yes[a]	No
(7) Graphite–Fe	Yes	No
(8) Graphite–Fe$_3$O$_4$	No	No
(9) Graphite–Fe–astronomical silicate	Yes	No
(10) Graphite–Fe$_3$O$_4$–astronomical silicate	Yes	Yes
(11) Graphite–Fe–Mg$_2$SiO$_4$	Yes	No
(12) Graphite–Fe$_3$O$_4$–Mg$_2$SiO$_4$	Yes	Yes
(13) Graphite–Fe–astronomical silicate–Mg$_2$SiO$_4$	Yes	No
(14) Graphite–Fe$_3$O$_4$–astronomical silicate–Mg$_2$SiO$_4$	Yes	Yes
(15) Graphite–FeS–astronomical silicate–Mg$_2$SiO$_4$	Yes	No

Notes. We count the species when its fraction is more than 10%.
[a] This model is ruled out if we consider the lack of 11.3 μm feature.

0, 0.1, and 0.4. (The curve for $f_{C,gra}/f_{Fe,asil} = 0.4$ appears to be out of the 1σ range, but it satisfies 1σ if $a_{max} \simeq 0.19\,\mu m$.) The model for $f_{C,gra}/f_{Fe,asil} \leqslant 0.4$ reproduces the SMC extinction curve within 1σ when q and a_{max} are adjusted. With $f_{C,gra}/f_{Fe,asil} = 0.4$ one sees in this figure the symptom that a small 2175 Å bump starts appearing and the rise toward the far-UV side becomes insufficient. We draw another curve (dot-dashed curve) with the minimum grain-size cutoff increased to $a_{min} = 0.02\,\mu m$, removing much of the small graphite grains. This curve lies similar to the one suggested by Calzetti et al. (1994) for star-forming galaxies. The bump at 2175 Å is reduced and becomes insignificant, but the removal of small size grains makes the far-UV rise insufficient. Therefore, such a case is excluded. Within the graphite–silicate model, the way to make the predicted extinction consistent with the observation is not to change the grain-size parameters but to decrease the abundance of graphite grains. The steeper rise toward the far-UV is accounted for by the smaller silicate grains.

The abundance of Si and C contained in dust is shown in Figure 15, where the abundance from Russell & Dopita (1992) is also indicated with dashed lines. We have $\log(Si/H) + 12 = 6.7$–7.8 and $\log(C/H) + 12 \leqslant 7.9$ from the extinction in the SMC. When $f_{Si,grain} = 1$, $\log(C/H) + 12 \leqslant 7.6$ in agreement with Equation (16) below. It is noted that the carbon abundance in graphite in the SMC is at least a factor of 1.5 times smaller than the abundance of Russell & Dopita (if Si is all condensed into dust; following the horizontal dashed line); the latter gives 7.73 for C and 7.03 for Si. The upper and lower curves correspond to the 1σ error of $N_H/E(B-V)$. For the SMC $\rho_{gra}/\rho_{asil} = 0.54\,f_{C,gra}/f_{Fe,asil} \leqslant 0.22$.

Figure 16 is a summary of the region of q and a_{max}, where the graphite–silicate model gives the extinction curve within the 1σ range marginalized over $f_{C,gra}/f_{Fe,asil}$. The allowed grain-size distribution again lies in $3.3 \lesssim q \lesssim 3.8$ and $0.19\,\mu m \lesssim a_{max} \lesssim 0.35\,\mu m$. It is interesting to observe that this range for the SMC agrees with that for the MW (recapitulated in the figure with the dotted curve) in spite of the significantly different behavior of the two extinction curves, as was noted earlier in Pei (1992).

The other curves in Figure 16 show the regions allowed by $N_H/E(B-V)$ for the 1σ error of Equation (2). The overlap of the two constraints is seen for

$$f_{C,gra} < 0.41. \qquad (16)$$

This allowed maximum fraction of graphite is smaller than the minimum $f_{C,gra}/f_{Fe,asil}$ favored for the MW ($f_{C,gra} \geqslant 0.56$), suggesting that condensation of carbon into grains should be less efficient in the SMC, as might be satisfied if, e.g., $f_{C,gra} \propto N_C$. More detailed arguments, however, depend on the accuracy of the abundance estimates, in particular, for the SMC.

For the model that satisfies 1σ constraints of both extinction curve and $E(B-V)$ size for the SMC, we find $\rho_{dust}/\rho_H = 1/760^{+150}_{-660}$, where the large error range comes from that of $E(B-V)/N_H$, and corresponds roughly to the upper and lower curves of the allowed region in Figure 15. If the abundance is constrained with Russell & Dopita's value and Fe is all condensed,

$$\rho_{dust}/\rho_H = 1/760^{+70}_{-90}. \qquad (17)$$

We have

$$K_{ext} = (2.2 \pm 0.3) \times 10^4 \text{ mag cm}^2 \text{ g}^{-1}. \qquad (18)$$

(It is $(2.1 \pm 0.4) \times 10^4$ mag cm^2 g^{-1} if the abundance constraints are removed.) The ratio of graphite to silicate is $\rho_{gra}/\rho_{asil} =$
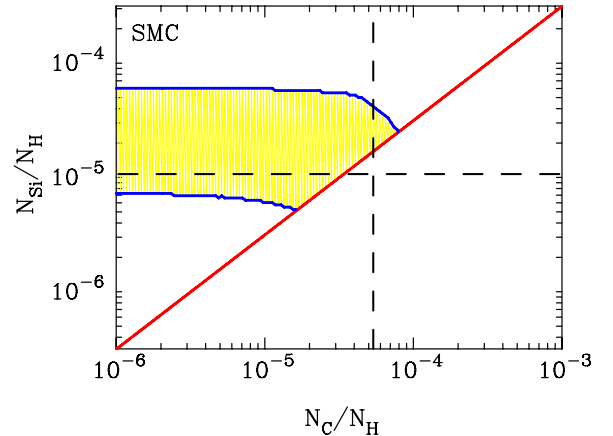

Figure 15. Abundance of C and Si in dust grains relative to hydrogen for the SMC to meet the extinction curve. The range left of the oblique line is allowed from the extinction curve, and that within the two curves running nearly horizontal is from $E(B-V)/N_H$. The two dashed lines (horizontal and vertical) show the total abundance of C and Si from Russell & Dopita (1992). (A color version of this figure is available in the online journal.)

0.11 ± 0.11, or $N_C/N_{Fe} = 1.6 \pm 1.6$, in numbers of atoms. This ratio is 4.5 times smaller than that for the MW. The abundance itself indicates the ratio of C/Fe to be 1.4 times smaller, so the formation of carbonaceous grains is suppressed by ≈ 3 times more in the SMC.

6. CONCLUSIONS AND DISCUSSION

We have confirmed that the graphite–silicate grain model gives a satisfactory description of the extinction curves within the *simple power-law model* of the size distribution. The grain-size distribution is tightly constrained to the index $q = 3.5 \pm 0.2$. We showed that departures from a power law are not needed. However, we need to cutoff the power law at some maximum size, $a = 0.2$–$0.3\,\mu m$. Grains may be a variety of carbonaceous and silicate materials. Their size parameters, however, vary little and the same parameters also apply to both MW and SMC extinction curves in spite of their apparently different behavior. The difference between the two extinction curves can be ascribed to the abundance of graphite relative to silicates, and hence to some lower efficiency ($\lesssim 1/2$) of graphite condensation, beyond the lower ratio ($\lesssim 1/1.5$) of carbon to silicon in the SMC indicated in abundance estimates currently available. We also remarked on the somewhat dissatisfying description of the 2175 Å feature.

While grains can be a variety of combinations that contain silicate and carbonaceous material, the presence of a significant abundance of graphite is important. It is interesting to note that the resulting $q = 3.5$ is the power expected from collisional equilibrium for small grains. We have derived the elemental abundance of Si and C contained in grains from the extinction. For the MW it is consistent with solar. If we take the widely adopted abundance of GS98, we infer the fraction of carbonaceous grains against total carbon, $f_{C,gra} = 0.6$–0.7, which agrees with the observational depression factor for carbon. This may be compared with the corresponding value for the SMC, $f_{C,gra} \lesssim 0.4$, taking the elemental abundance of Russell & Dopita (1992). The required silicate is also consistent.

The upper cutoff is compelling for the grain-size distribution to give the correct shape of the extinction curve. Extending it to a larger size would disrupt the agreement with observations (see Draine 2009): for example, the R_V parameter becomes
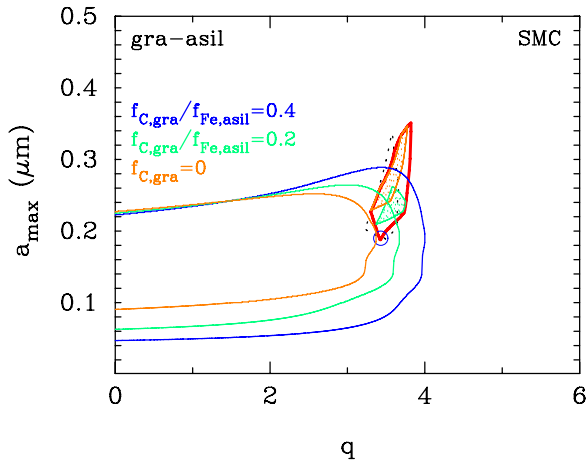
Figure 16. Allowed regions of q and a_{max} with which the model satisfies the "1σ" extinction ranges for the SMC. The graphite-to-silicate ratio is marginalized over $0 \leqslant f_{C,gra}/f_{Fe,asil} \leqslant 0.41$. The inlaid curves indicate the regions for $f_{C,gra} = 0$, 0.2, and 0.4. The regions for 0.4 is a point indicated with a small circle (the actual region is enlarged) near the bottom of the allowed region. The constraints from the reddening $E(B - V)/N_H$ are shown with brown, green, and blue contours for $f_{C,gra} = 0$, 0.2, and 0.4 ($f_{Fe,asil} = 1.0$). The thin dotted curve recapitulates the allowed region for MW dust in Figure 6 for comparison.

intolerably large.[14] While we are not able to find the reason for the cutoff, we may see another argument that forces us to impose the presence of a cutoff in the power law. The abundance of grains is constrained at a submicrometer region by the amount of the observed optical extinction. The power law with $q = 3.5$ means that the integrated mass of grains is slowly increasing with the upper cutoff mass m_c as $m_c^{0.17}$. If the cutoff were larger, we would have too large a mass in grains to be accounted for as a product of stellar evolution. The dust mass density relative to hydrogen $\rho_{dust}/\rho_H \approx 0.008$ means $\Omega_{dust} \approx 4.4 \times 10^{-6}$ taking the global hydrogen abundance for H I and H$_2$ observations, $\Omega_H = 5.4 \times 10^{-4}$. If dust is a product of stellar evolution over cosmic time, stars of the amount $\Omega_{star} \simeq 0.003$ would produce dust grains no more than $\Omega_{dust} \approx 1 \times 10^{-5}$ (Fukugita 2011). This amount is consistent with the power-law distribution constrained from the extinction if the power law cutoff is at $0.25\,\mu$m. If the maximum size cutoff were an order of magnitude larger, say, the dust abundance would be larger by $\approx 50\%$, more than the star formation activity can account for.

Small astronomical objects may also obey the same power law. Their normalization, however, should be smaller by a large factor than that for the dust grains. The integrated mass density of the core of planets for $a > 100$ km is estimated to be 1/300 that of dust grains (Fukugita 2011). The power law should be broken by two orders of magnitude at a few tenths of a micrometer. The addition of the planet core mass disturbs little the estimate of the mass density borne by small objects.

We have emphasized that the behavior of the extinction curve in NIR is important. If the power of the NIR extinction curve $\lambda^{-\gamma}$ is as small as $\gamma = 1.6$, as was derived earlier and adopted by CCM or WD01, one cannot reproduce the extinction curve from UV to NIR by the grain model with a simple power law of the grain size. One needs to substantially adjust the size distribution, by, e.g., adding extra components, as was done by WD01, Zubko et al. (2004), and others. With a larger power of

the NIR wavelength dependence, such as $\gamma = 1.8$–2.1, however, the simple power-law model works for the observed extinction. The NIR power $\gamma = 1.6$ can be consistent with the power-law grain size only when the iron component of grains is largely in magnetite, which has a large NIR scattering efficiency.

We have seen that the presence of graphite grains is uniquely important, at least in the MW, although the condensation of C atoms may not necessarily be all into graphite. Roughly half the amount of carbon may be condensed into a glassy or an amorphous phase, whereas some significant fraction of C atoms must be in graphite. Iron may also remain in the metallic phase. There is no need for all Fe atoms to be locked in astronomical silicate. The effective ratio of Mg to Fe in olivine seems arbitrary. Fe$_3$O$_4$, however, cannot be predominant. Fe may also be in troilite, as much as the sulfur abundance allows.

The size distribution is well converged to a narrow range, regardless of whether other grain compositions are included. The variation of extinction along lines of sight may be accounted for by a small variation of the grain-size distribution with $\Delta q \approx 0.2$ and/or $\Delta a_{max}/a_{max} \approx 0.3$, and with changing the graphite to silicate ratio as for the difference between the MW and the SMC. It is noteworthy that the $a^{-3.5}$ power as expected in collisional equilibrium seems to be generic to dust grains.

REFERENCES

Anders, E., & Grevesse, N. 1989, GeCoA, 53, 197
Asplund, M., Grevesse, N., Sauval, A. J., & Scott, P. 2009, ARA&A, 47, 481
Biermann, P., & Harwit, M. 1980, ApJL, 241, L105
Bohlin, R. C., Savage, B. D., & Drake, J. F. 1978, ApJ, 224, 132
Caffau, E., Ludwig, H.-G., Steffen, M., Freytag, B., & Bonifacio, P. 2011, SoPh, 268, 255
Calzetti, D., Kinney, A. L., & Storchi-Bergmann, T. 1994, ApJ, 429, 582
Cardelli, J. A., Clayton, G. C., & Mathis, J. S. 1989, ApJ, 345, 245 (CCM)
Cardelli, J. A., Meyer, D. M., Jura, M., & Savage, B. D. 1996, ApJ, 467, 334
Cartledge, S. I. B., Clayton, G. C., Gordon, K. D., et al. 2005, ApJ, 630, 355
Chiar, J. E., & Tielens, A. G. G. M. 2006, ApJ, 637, 774
Choyke, W. J., & Palik, E. D. 1985, in Handbook of Optical Constants of Solids, ed. E. D. Palik (San Diego, CA: Academic), 587
Clayton, G. C., Gordon, K. D., Salama, F., et al. 2003a, ApJ, 592, 947
Clayton, G. C., Gordon, K. D., & Wolff, M. J. 2000, ApJS, 129, 147
Clayton, G. C., Wolff, M. J., Sofia, U. J., Gordon, K. D., & Misselt, K. A. 2003b, ApJ, 588, 871
Dohnanyi, J. S. 1969, JGR, 74, 2531
Dorschner, J. 1982, Ap&SS, 81, 323
Dorschner, J., Begemann, B., Henning, Th., Jäger, C., & Mutschke, H. 1995, A&A, 300, 503
Draine, B. T. 2003a, ARA&A, 41, 241
Draine, B. T. 2003b, ApJ, 598, 1026
Draine, B. T. 2009, SSRv, 143, 333
Draine, B. T., & Lee, H. M. 1984, ApJ, 285, 89 (DL84)
Draine, B. T., & Malhotra, S. 1993, ApJ, 414, 632
Edoh, O. 1983, PhD thesis, Univ. Arizona
Fitzpatrick, E. L., & Massa, D. 2007, ApJ, 663, 320 (FM07)
Fitzpatrick, E. L., & Massa, D. 2009, ApJ, 699, 1209
Fritz, T. K., Gillessen, S., Dodds-Eden, K., et al. 2011, ApJ, 737, 73
Fukugita, M. 2011, arXiv:1103.4191
Gordon, K. D., Clayton, G. C., Misselt, K. A., Landolt, A. U., & Wolfe, M. J. 2003, ApJ, 594, 279 (G03)

---

[14] This is caused by the fact that the R_V parameter resulting from silicate grains is wildly oscillating as a function of a for $a > 0.2\,\mu$m, which makes the resulting R_V parameter too large.

Grevesse, N., & Sauval, A. J. 1998, SSRv, 85, 161 (GS98)
Gudennavar, S. B., Bubbly, S. G., Preethi, K., & Murthy, J. 2012, ApJS, 199, 8
Hellyer, B. 1970, MNRAS, 148, 383
Joblin, C., Léger, A., & Martin, P. 1992, ApJL, 393, L79
Kim, S.-H., Martin, P. G., & Hendry, P. D. 1994, ApJ, 422, 164
Lodders, K. 2010, Principles and Perspectives in Cosmochemistry, Astronomy and Space Science Proceedings (Berlin: Springer), 379
Martin, P. G., & Whittet, D. C. B. 1990, ApJ, 357, 113
Mathis, J. S., & Cardelli, J. A. 1992, ApJ, 398, 610
Mathis, J. S., Rumpl, W., & Nordsieck, K. H. 1977, ApJ, 217, 425 (MRN)
Nieva, M.-F., & Przybilla, N. 2012, A&A, 539, 143
Pan, M., & Sari, R. 2005, Icar, 173, 342
Pei, Y. C. 1992, ApJ, 395, 130
Rieke, G. H., & Lebofsky, M. J. 1985, ApJ, 288, 618
Russell, S. C., & Dopita, M. A. 1992, ApJ, 384, 508

Semenov, D., Henning, Th., Helling, Ch., Ilgner, M., & Sedlmayr, E. 2003, A&A, 410, 611
Sofia, U. J., Lauroesch, J. T., Meyer, D. M., & Cartledge, S. I. B. 2004, ApJ, 605, 272
Sofia, U. J., Parvathi, V. S., Babu, B. R. S., & Murthy, J. 2011, AJ, 141, 22
Stecher, T. P., & Donn, B. 1965, ApJ, 142, 1681
Toon, O. B., Pollack, J. B., & Khare, B. N. 1976, JGR, 81, 5733
Tumlinson, J., Shull, J. M., Rachford, B. L., et al. 2002, ApJ, 566, 857
Weingartner, J. C., & Draine, B. T. 2001, ApJ, 548, 296 (WD01)
Welty, D. E., Xue, R., & Wong, T. 2012, ApJ, 745, 173
Whittet, D. C. B., Duley, W. W., & Martin, P. G. 1990, MNRAS, 244, 427
Winkler, H. 1997, MNRAS, 287, 481
York, D. G., Khare, P., Vanden Berk, D., et al. 2006, MNRAS, 367, 945
Zubko, V., Dwek, E., & Arendt, R. G. 2004, ApJS, 152, 211
Zubko, V. G., Mennella, V., Colangeli, L., & Bussoletti, E. 1996, MNRAS, 282, 1321